Disturbance-Observer-Based Control of DFIG in Island Mode for Microgrid Applications

ADNAN OSMANOVIĆ[1], **(Member, IEEE), TARIK UZUNOVIĆ**[1], **(Senior Member, IEEE),**
ASIF ŠABANOVIĆ[2], **(Life Senior Member, IEEE), AND JASMIN VELAGIĆ**[1], **(Member, IEEE)**
[1]Faculty of Electrical Engineering, University of Sarajevo, 71000 Sarajevo, Bosnia and Herzegovina
[2]Faculty of Engineering and Natural Sciences, International University of Sarajevo, 71210 Sarajevo, Bosnia and Herzegovina

Corresponding author: Adnan Osmanović (adnan.osmanovic@etf.unsa.ba)

ABSTRACT This paper introduces a novel control approach for Doubly-Fed Induction Generator (DFIG) operating in island mode based on the cascaded control structure with disturbance estimation. The control of the DFIG is a challenging task due to its inherent nonlinearity, fast dynamics, and unpredictable disturbances acting on the system. The proposed control structure involves a nominal controller for plant and disturbance observer (DOB) in each of the inner and outer control loop. The first-order disturbance observers are designed to estimate the time-varying and unknown disturbances. With disturbance estimation, the nominal linear dynamics is obtained in both loops. This enables the same approach for designing controllers for the inner and outer loop which significantly simplifies implementation. The controllers are designed based on the demanded error dynamics and ensure stable operation of the system, while proposed DOBs estimate disturbances including external load. Finally, the effectiveness and quality of the proposed control structure were verified through numerical simulations in terms of external disturbances rejection and closed-loop tracking performance.

INDEX TERMS Disturbance observer, DFIG, microgrid, renewable energy, wind energy conversion system, island mode operation.

I. INTRODUCTION

Renewable energy sources (RES) have become an inevitable part of modern microgrids. The most important control requirements for these energy sources are their stable operation and efficient integration of RES in the energy system, especially when operating in islanded mode, such as microgrid applications where weak grid conditions impose frequency and voltage regulation for all energy sources. The doubly-fed induction generators (DFIG) are the most widely employed in wind energy conversion systems (WECS) [1]. They provide a variable speed operation as well as decoupled active and reactive power control. This type of generator can be used in various types of primary movers. In addition to WECS, DFIG has been used for internal combustion engines [2] and water turbines [3]. Further improvements in the efficiency, stability, easier integration and synchronization with the grid, and a quality improvement of the

produced energy depend on the efficiency of control structures for DFIG-based systems. The field-oriented control (FOC) [4], [5], can be applied to the DFIG generator [6]. Aligning with the stator voltage allows easy relationship between currents and power [7]–[9], where the d and q components of the stator current are proportional to the active and reactive power of the generator [10]. Sensorless FOC control of DFIG generator based on the reference model observer is presented in [11]. The FOC system using the neural discrete control in the sliding mode for active and reactive power control was proposed in [12], where the performance of this system, in terms of robustness to unknown interference with DFIG generator connected to the grid, was considered. The vector control of the DFIG generator based on the direct current vector was realized in [13].

An alternative approach to the FOC-based control of DFIG generator represents a direct torque control (DTC) [14]. In this approach, the stator flux and electromagnetic torque are directly controlled using lookup tables. However, this type of control strategy has some drawbacks, such as high

The associate editor coordinating the review of this manuscript and approving it for publication was Mehrdad Saif[ID].

torque pulsations, variable switching frequency in power converters, and difficulties related to torque and flux control at low speeds.

The direct power control (DPC) technique was originally proposed for controlling three-phase PWM rectifiers [15]–[17].

In [18] and [19] the control structures based on DPC for DFIG generator under unbalanced grid voltage are proposed. For removing the difficulties associated with the rotor flux estimation, another method based on DPC is proposed in [20]. The work [21] presents a similar control method that is based on DPC but without using rotor position sensor. In [22], DPC method to limit the rotor voltage is proposed to improve the system transient performance.

Several nonlinear control methods and techniques have been designed to mitigate issues of sub-synchronous control interaction for DFIG based wind power plants [23], [24]. When DFIG operates in the grid-connected mode, the control objective is related to active and reactive power that generator delivers to the grid. The majority of the proposed control methods for the DFIG are intended to use in the grid-connected mode operation. However, these controllers need changes in order to provide voltage and frequency regulation in stand-alone mode [25]. On the other hand, the control objective for the DFIG in the island mode is related to stable voltage and frequency generation on the stator side. In general, there are two main control strategies for DFIG in island mode operation: stator flux-oriented methods and methods based on direct voltage control (DVC). In [26], one of the rotor current components is employed to control the machine flux while other is used to maintain reference frame orientation. The stator flux-based control methods for the DFIG without the rotor position sensor are introduced in [27]–[29], while the control structures based on DVC are proposed in [30]–[33]. This control method is based on the equivalent circuit model of DFIG in the synchronous reference frame. It is capable of simultaneous control of the output stator voltage magnitude and frequency of the DFIG system [34]. Several methods based on DOB have been proposed to overcome problems with model dependencies and external interference for islanded mode operation of DFIG. In [35] is presented direct stator voltage control scheme based on the second-order auto-disturbance rejection control (ADRC) for the rotor side converter of DFIG. This method suppress the disturbances caused by the DFIG parameters, however main shortcomings are voltage ripple at the output. In [36] is proposed cascaded control structure with PI controllers and compensation terms in both outer and inner control loop.

This work extends cascaded PI control method applied to DFIG by introducing DOBs in both inner and outer loops. It reduces the controller effort and significantly improves performance of the overall system as well as control performance in each control loop. The proposed method compensates disturbance terms and simplifies controller design, since compensated controlled plant is a linear first order system. Therefore, it differs from the other DOB-based methods

for DFIG in island mode operation, since it unifies controller design methodology in both loops. To the best of our knowledge, the existing cascaded control systems for DFIG which includes observers in each loops has not been proposed yet. Furthermore, this paper illustrates a number of benefits of the proposed design technique from the engineering perspective. It results in the control feedback law with simple first-order filters and low computation requirements. Moreover, the introduced method facilitates controller design procedure with consistent control structures in all control loops. It means that only one gain and cutoff frequency per loop is adjusted, while the other gains depend on DFIG parameters. These can be easily obtained by standard short and open circuit experiment. Unlike the method presented in [36], in which disturbance terms are calculated under assumption that all system dynamics is modeled and known, the proposed control system estimates disturbances. This results in the better disturbance rejection, especially when system is subjected to unknown external disturbances.

This paper is organized as follows. Section II describes the system based on the DFIG that operates in island mode. In Section III, a design of the proposed control system is presented. Simulation results are given in Sections IV. Section V concludes the paper and discusses future extensions of the proposed control system.

II. SYSTEM DESCRIPTION

In this section, the overall control system for wind-driven DFIG as renewable energy source (RES) that supplies an isolated load or microgrid, will be described. The basic structure of this system is illustrated in Fig.1. The proposed controllers are going to be subjects of consideration in the next section.
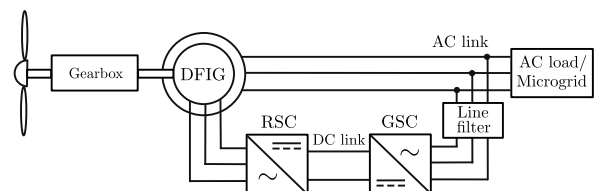

FIGURE 1. The system under consideration-DFIG connected to microgrid.

When RES works in standalone or island operation mode it must satisfy both AC load nominal voltage and frequency. This operation mode is very important, especially if the microgrid is located in areas without any possibility to be connected to the utility grid.

The DFIG model in a three-phase coordinate system, considering the symmetrical wound induction machine is described by the following equations [37]

$$\mathbf{v}_s = \mathbf{R}_s \mathbf{i}_s + \frac{d\Psi_s}{dt} \tag{1}$$

$$\mathbf{v}_r = \mathbf{R}_r \mathbf{i}_r + \frac{d\Psi_r}{dt} \tag{2}$$

$$\frac{J}{p} \frac{d\omega_r}{dt} = T_{pm} - T_e \tag{3}$$

$$T_e = p \cdot \mathbf{i}_s^\top \cdot \frac{d\mathbf{L}_{sr}}{dt} \cdot \mathbf{i}_r \tag{4}$$

$$\frac{d\theta_r}{dt} = \omega_r. \tag{5}$$

The stator and rotor flux linkages are expressed as

$$\Psi_s = \mathbf{L}_s \mathbf{i}_s + \mathbf{L}_{sr} \mathbf{i}_r \tag{6}$$

$$\Psi_r = \mathbf{L}_r \mathbf{i}_r + \mathbf{L}_{rs} \mathbf{i}_s \tag{7}$$

where $\mathbf{v}_s = [v_{sa} \ v_{sb} \ v_{sc}]^\top$ and $\mathbf{v}_r = [v_{ra} \ v_{rb} \ v_{rc}]^\top$ are respectively the stator and the rotor voltage vectors; $\mathbf{i}_s = [i_{sa} \ i_{sb} \ i_{sc}]^\top$ and $\mathbf{i}_r = [i_{ra} \ i_{rb} \ i_{rc}]^\top$ are the stator and the rotor current vectors; $\Psi_s = [\Psi_{sa} \ \Psi_{sb} \ \Psi_{sc}]^\top$ and $\Psi_r = [\Psi_{ra} \ \Psi_{rb} \ \Psi_{rc}]^\top$ are stator and rotor flux linkage vectors; $\mathbf{R}_s = \mathrm{diag}(R_{sa}, R_{sb}, R_{sc}) = \mathrm{diag}(R_s, R_s, R_s)$ and $\mathbf{R}_r = \mathrm{diag}(R_{ra}, R_{rb}, R_{rc}) = \mathrm{diag}(R_r, R_r, R_r)$ are stator and rotor winding resistance matrices; ω_r is the electrical angular speed of the rotor; T_e is the electromagnetic torque; T_{pm} is the prime mover torque; J is the inertia torque and p is number of pairs of poles. Matrices $\mathbf{L}_s$ and $\mathbf{L}_r$ are respectively the stator and the rotor winding inductance matrices; $\mathbf{L}_{sr}$ and $\mathbf{L}_{rs}$ are matrices of the mutual inductances between stator and rotor windings. Determination of the inductance matrices $\mathbf{L}_s$, $\mathbf{L}_r$, $\mathbf{L}_{sr}$ and $\mathbf{L}_{rs}$ is described in detail in [37].

In order to complete the system model described by (1)-(7) it is necessary to include the equation for the stator voltage. The stator voltage for loaded generator could be calculated as

$$\mathbf{u}_s = -\mathbf{Z}_l \mathbf{i}_s \tag{8}$$

where $\mathbf{Z}_l$ is diagonal matrix of per-phase loads $\mathbf{Z}_l = \mathrm{diag}(Z_{l1}, Z_{l2}, Z_{l3})$.

III. CONTROL SYSTEM DESIGN

The control system is designed in rotating *dq* reference frame that rotates with angular speed denoted with ω_1. Using Clarke and Park transformation, all three-phase quantities were transformed to *dq* reference frame.

In the island mode operation, the stator voltage must comply to the load specifications. Thus, the main control task will be to maintain a stable stator voltage and frequency. For this purpose, the controller will include virtual three phase symmetrical reference that rotates with angular frequency $\omega_1 = 2\pi f_1$. This will ensure a consistent base for all transformations. It has to be noted that f_1 could be arbitrarily selected; therefore, the output voltage frequency can be changed.

For obtaining the transformation angle for Clarke and Park transformations from *abc* to *dq* reference frame, phase locked loop (PLL) algorithm is used.

In Fig.2, signals v_a, v_b and v_c denote virtual three-phase system components. Since our work is considering island mode of operation, this signals are generated internally by controller. In the case of grid-connected mode these are obtained by measurements e.g. voltages at the point of synchronization.

Fig. 3 illustrates the vector diagram of the virtual reference frame and its component v_d, as well as the stator space
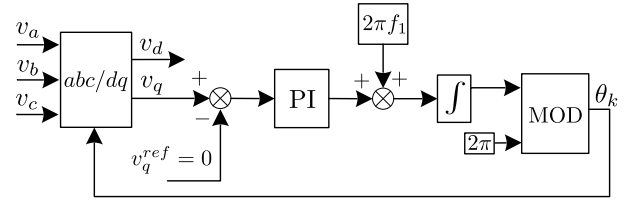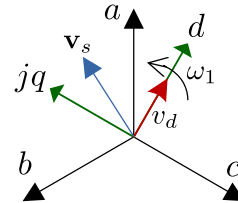

FIGURE 2. Structure of implemented PLL algorithm.

FIGURE 3. Vector of the stator voltage v_s in *dq* reference frame.

vector $\mathbf{v}_s$. It is important to mention that angular speed ω_1 of *dq* frame is chosen to be same as angular speed of $\mathbf{v}_s$. That means, components of $\mathbf{v}_s$ will have constant values v_{sd} and v_{sq} in the considered reference frame. Space vectors in *dq* frame are represented as complex quantities e.g. $\mathbf{f} = f_d + jf_q$, where $j = \sqrt{-1}$.

The mathematical model of the DFIG in the rotating *dq* reference frame is described by (all rotor quantities are referred on the stator side)

$$\mathbf{v}_s = R_s \mathbf{i}_s + \frac{d\Psi_s}{dt} + j\omega_1 \Psi_s \tag{9}$$

$$\mathbf{v}_r = R_r \mathbf{i}_r + \frac{d\Psi_r}{dt} + j(\omega_1 - \omega_r)\Psi_r \tag{10}$$

$$\Psi_s = L_{s\sigma} \mathbf{i}_s + L_\mu(\mathbf{i}_s + \mathbf{i}_r) = L_s \mathbf{i}_s + L_\mu \mathbf{i}_r \tag{11}$$

$$\Psi_r = L_{r\sigma} \mathbf{i}_r + L_\mu(\mathbf{i}_s + \mathbf{i}_r) = L_\mu \mathbf{i}_s + L_r \mathbf{i}_r \tag{12}$$

$$L_s = L_\mu + L_{s\sigma}, \quad L_r = L_\mu + L_{r\sigma} \tag{13}$$

$$J\frac{1}{p}\frac{d\omega_r}{dt} = T_{pm} - T_e \tag{14}$$

$$T_e = \frac{3}{2} p \frac{L_e}{L_{s\sigma} L_{r\sigma}} \left(\psi_{sq}\psi_{rd} - \psi_{sd}\psi_{rq}\right) \tag{15}$$

where L_μ is mutual inductance, $L_{s\sigma}$ and $L_{r\sigma}$ are the stator and rotor leakage inductance; ω_1 is the electrical angular speed of the *dq* reference frame given by $\omega_1 = 2\pi f_1$ and ω_r is the electrical angular speed of the rotor. The constant parameter L_e is defined with

$$\frac{1}{L_e} = \frac{1}{L_\mu} + \frac{1}{L_{s\sigma}} + \frac{1}{L_{r\sigma}}. \tag{16}$$

If we eliminate stator current in (11) with relation (8) and insert equation of stator voltage dynamics (9) into (11) we have

$$L_s \dot{\Psi}_s + (\mathbf{Z}_l + R_s + j\omega_1 L_s) \Psi_s = L_\mu (\mathbf{Z}_l + R_s) \mathbf{i}_r. \tag{17}$$

From (17) we can notice that stator flux can be controlled with the rotor current. However, the dynamics of the rotor

current is controlled by the input rotor voltage. Thus, a cascaded control structure can be utilized. Within the structure, the internal rotor current control loop will be created, while the outer loop will control the stator flux and it will provide a reference for the internal current loop. The basic idea of the structure is illustrated in Fig. 4.
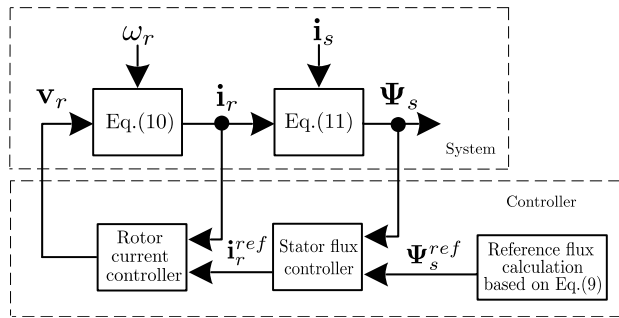

FIGURE 4. Structure of DFIG system with feedback control.

Considering (9), that defines the components of the stator voltage in steady state, one can calculate references for the stator flux components as follows

$$v_{sd} = R_s i_{sd} - \omega_1 \Psi_{sq} \rightarrow \Psi_{sq}^{ref} = \frac{1}{\omega_1}\left(R_s i_{sd} - v_{sd}^{ref}\right) \quad (18)$$

$$v_{sq} = R_s i_{sq} + \omega_1 \Psi_{sd} \rightarrow \Psi_{sd}^{ref} = \frac{1}{\omega_1}\left(v_{sq}^{ref} - R_s i_{sq}\right) \quad (19)$$

Reference flux calculation block actually implements (18) and (19).

The controller of the rotor currents will be designed using an observer-based cascaded structure. The inner loop will control the rotor currents, and the outer control loop will serve as the estimator of the rotor current set point. This set point of the rotor currents depends on the load and demanded stator voltage. For both loops, the proposed control structure contains two components: (i) a disturbance observer which estimates and compensates the total disturbance in the controlled plant, (ii) a nominal plant controller, where the nominal plant denotes the controlled plant with compensated disturbance. The first component cancels the influence of the disturbance, while the second controls the obtained nominal plant; therefore, the total control input will be sum of the outputs of these components.

Inserting (12) to (10) yields:

$$L_r \frac{d\mathbf{i}_r}{dt} = \mathbf{v}_r - \underbrace{R_r \mathbf{i}_r + L_\mu \frac{d\mathbf{i}_s}{dt} + j(\omega_1 - \omega_r)\mathbf{\Psi}_r}_{\mathbf{v}_r^{dist}} \quad (20)$$

$$L_r \frac{d\mathbf{i}_r}{dt} = \mathbf{v}_r - \mathbf{v}_r^{dist}. \quad (21)$$

The disturbance term $\mathbf{v}_r^{dist}$ can be estimated using first order disturbance observer [38] with cutoff frequency g_c

$$\hat{\mathbf{v}}_r^{dist} = (\mathbf{v}_r - L_r g_c \mathbf{i}_r) Q_c - L_r g_c \mathbf{i}_r \Leftrightarrow \hat{\mathbf{v}}_r^{dist} = Q_c \mathbf{v}_r^{dist} \quad (22)$$

where $Q_c = g_c/(s + g_c)$ is a first-order low-pass filter.

Let us now assume that control input $\mathbf{v}_r$ is composed as

$$\mathbf{v}_r = \mathbf{v}_r^{nom} + \hat{\mathbf{v}}_r^{dist} \quad (23)$$

where $\mathbf{v}_r^{nom}$ is the control input for the nominal plant with compensated disturbance $\mathbf{v}_r^{dist}$. The dynamics of the nominal plant becomes

$$\frac{d\mathbf{i}_r}{dt} = \frac{1}{L_r}\mathbf{v}_r^{nom} - (1 - Q_c)\mathbf{v}_r^{dist} \quad (24)$$

In the discussed dynamics, $\mathbf{v}_r^{dist}$ is a low-frequency signal due to the selected dq frame of reference. Therefore, the term $(1 - Q_c)$ is very close to zero in the frequency range of interest, and dynamics (24) becomes

$$\frac{d\mathbf{i}_r}{dt} = \frac{1}{L_r}\mathbf{v}_r^{nom} \quad (25)$$

The error between the reference and actual rotor current and its dynamics are given by

$$\mathbf{e} = \mathbf{i}_r^{ref} - \mathbf{i}_r \quad (26)$$

$$\dot{\mathbf{e}} = \dot{\mathbf{i}}_r^{ref} - \dot{\mathbf{i}}_r = \dot{\mathbf{i}}_r^{ref} - \frac{1}{L_r}\mathbf{v}_r^{nom} \quad (27)$$

where $\mathbf{i}_r^{ref}$ is the reference current and $\mathbf{i}_r$ denotes actual value of the rotor current in the dq frame. The nominal control input

$$\mathbf{v}_r^{nom} = L_r \left(\dot{\mathbf{i}}_r^{ref} + \mathbf{K}_r \cdot \mathbf{e}\right). \quad (28)$$

where matrix $\mathbf{K}_r$ has as diagonal entries the controller gains, i.e., $\mathbf{K}_r = \text{diag}(K_{rd}, K_{rq})$, yields the error dynamics

$$\dot{\mathbf{e}} + \mathbf{K}_r \cdot \mathbf{e} = \mathbf{0}. \quad (29)$$

Dynamics (29) shows that error is exponentially converging to zero for the control input defined by (23).

The outer control loop will be designed in order to obtain rotor current reference needed for achieving stable voltage and frequency generated at the stator of the DFIG. Previously designed, inner control loop controller enforces $\mathbf{i}_r \rightarrow \mathbf{i}_r^{ref}$, so we use $\mathbf{i}_r = \mathbf{i}_r^{ref}$ for the outer control loop design.

If we rearrange (17) we have

$$\tau_s \frac{d\mathbf{\Psi}_s}{dt} + \mathbf{\Psi}_s = L_\mu \left(\mathbf{i}_r^{ref} - \mathbf{i}_r^{dist}\right). \quad (30)$$

where $L_\mu \mathbf{i}_r^{dist} = L_\mu \frac{\mathbf{Z}_l}{R_s}\mathbf{i}_r - \frac{\mathbf{Z}_l}{R_s}\mathbf{\Psi}_s - j\omega_1\mathbf{\Psi}_s\tau_s$ and $\tau_s = \frac{L_s}{R_s}$.

From (30), the disturbance term $\mathbf{i}_r^{dist}$ can be estimated using the first-order disturbance observer [38] with cutoff frequency g_s as follows

$$\hat{\mathbf{i}}_r^{dist} = \left(\mathbf{i}_r^{ref} - \frac{\mathbf{\Psi}_s}{L_\mu} + \frac{\tau_s g_s}{L_\mu}\mathbf{\Psi}_s\right) Q_s - \frac{\tau_s g_s}{L_\mu}\mathbf{\Psi}_s \quad (31)$$

which in fact implements $\hat{\mathbf{i}}_r^{dist} = Q_s \mathbf{i}_r^{dist}$ where $Q_s = g_s/(s + g_s)$ is a low-pass filter.

It is important to notice that disturbance term $\mathbf{i}_r^{dist}$ also includes load impedance, which means that proposed DOB will compensate variations of the load impedance.
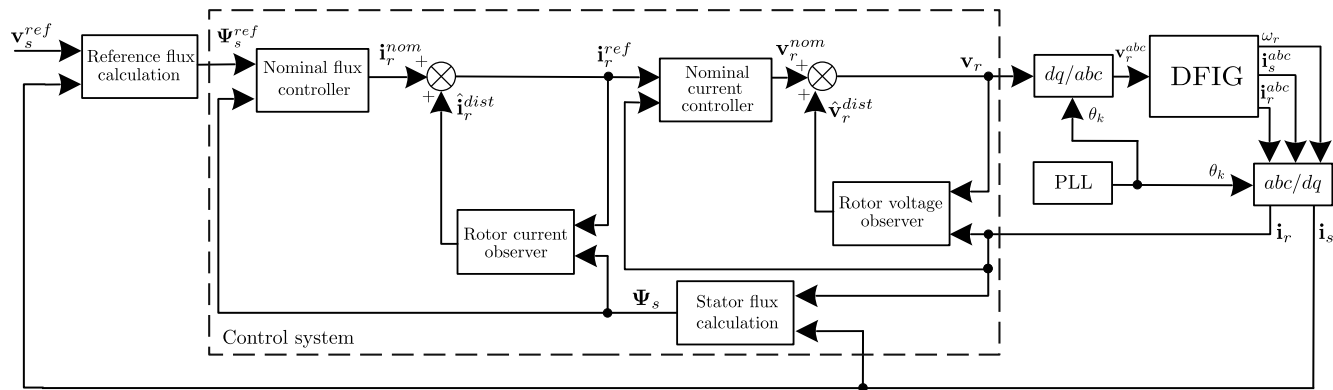
FIGURE 5. Proposed cascaded control system structure with nominal controllers and disturbance observers in each control loop.

Therefore, the controller does not require exact information about the external load.

If the control input $\mathbf{i}_r^{ref}$ is

$$\mathbf{i}_r^{ref} = \mathbf{i}_r^{nom} + \hat{\mathbf{i}}_r^{dist} \qquad (32)$$

where $\hat{\mathbf{i}}_r^{dist}$ is the estimated disturbance current and $\mathbf{i}_r^{nom}$ is the control input of the nominal plant with the disturbance compensated, system (30) becomes

$$\tau_s \frac{d\boldsymbol{\Psi}_s}{dt} + \boldsymbol{\Psi}_s = L_\mu \mathbf{i}_r^{nom} - L_\mu (1 - Q_s) \mathbf{i}_r^{dist}. \qquad (33)$$

In the discussed dynamics, $\mathbf{i}_r^{dist}$ is a low-frequency signal due to the selected dq frame of reference. Therefore, the term $(1 - Q_s)$ is very close to zero in the frequency range of interest, and dynamics (33) becomes

$$\tau_s \frac{d\boldsymbol{\Psi}_s}{dt} + \boldsymbol{\Psi}_s = L_\mu \mathbf{i}_r^{nom} \qquad (34)$$

The error between reference and actual stator flux and its dynamics are

$$\mathbf{e}_s = \boldsymbol{\Psi}_s^{ref} - \boldsymbol{\Psi}_s \qquad (35)$$

$$\dot{\mathbf{e}}_s = \dot{\boldsymbol{\Psi}}_s^{ref} - \dot{\boldsymbol{\Psi}}_s = \dot{\boldsymbol{\Psi}}_s^{ref} - \frac{L_\mu}{\tau_s}\mathbf{i}_r^{nom} + \frac{1}{\tau_s}\boldsymbol{\Psi}_s \qquad (36)$$

where $\boldsymbol{\Psi}_s^{ref}$ is the reference flux vector and $\boldsymbol{\Psi}_s$ denotes actual value of the stator flux components in dq reference frame. For

$$\mathbf{i}_r^{nom} = \frac{1}{L_\mu}\left(\boldsymbol{\Psi}_s + \tau_s\dot{\boldsymbol{\Psi}}_s^{ref} + \tau_s\mathbf{K}_s\mathbf{e}_s\right) \qquad (37)$$

where $\mathbf{K}_s$ is the diagonal matrix of controller gains $\mathbf{K}_s = \text{diag}(K_{sd}, K_{sq})$, the error dynamics becomes

$$\dot{\mathbf{e}}_s + \mathbf{K}_s \cdot \mathbf{e}_s = \mathbf{0}. \qquad (38)$$

The controller objective is to ensure stable voltage and frequency of the generated stator voltage. Since this objective is accomplished through direct control of the stator flux, it is necessary to define the relationship between the stator voltage and the stator flux in the steady state. This relationship is defined in (18) and (19).

The proposed control system structure is shown in Fig. 5 where all electrical quantities that are denoted with superscript abc are in the three phase system, all other are in dq rotating frame. One of the major advantages of the proposed controller is the same structure of the inner and outer loop, as well as the same systematic approach for the design of disturbance observers in these loops.

Reference flux calculation block implements (18) and (19) where $\mathbf{v}_s^{ref} = [v_{sd}^{ref} \quad v_{sq}^{ref}]^\top$ and $\boldsymbol{\Psi}_s^{ref} = [\Psi_{sd}^{ref} \quad \Psi_{sq}^{ref}]^\top$. Nominal flux controller is designed to control compensated plant (34) where $\boldsymbol{\Psi}_s^{ref}$ is calculated value of demanded flux that is related to the set point of the stator voltage $\mathbf{v}_s^{ref}$ and actual value of the stator current $\mathbf{i}_s$, which depends on the load connected to the stator of the generator. The output of this controller is $\mathbf{i}_r^{nom}$ that is actually control effort for compensated plant given by (37).

The rotor current observer estimates disturbance term denoted as $\mathbf{i}_r^{dist}$. This part of the proposed control system provides estimate of the disturbance $\hat{\mathbf{i}}_r^{dist}$ and it is obtained from (31). As the final output of the outer control loop is formed reference vector of rotor currents $\mathbf{i}_r^{ref}$. This output represents the set point for the inner control loop.

The inner control loop is designed to control rotor currents $\mathbf{i}_r$ and it is, as well as the outer (stator flux) control loop, designed based on the disturbance observer. In this case, the rotor voltage observer estimates rotor voltage disturbance denoted in (20) as $\mathbf{v}_r^{dist}$. The estimation of this term is implemented as (22) and estimated term is denoted as $\hat{\mathbf{v}}_r^{dist}$. The nominal current controller is designed to control the compensated plant (24) and its control output $\mathbf{v}_r^{nom}$ is given by (28). Finally, the input rotor voltage $\mathbf{v}_r$ is obtained from (23).

It is very important to note the following. The proposed cascaded control structure enables operation of DFIG in grid-connected mode. This type of operation requires only changes of quantities in the reference flux calculation. To be specific, the stator voltage in this operation mode is determined by the grid, while the reference stator flux is calculated based on reference and measured active and reactive power. In that case, the outer loop again calculates the rotor current

reference based on the desired and measured powers, while the structure of the flux and current loops remains exactly the same. Therefore, the proposed control structure gives a possibility for application in the island mode, as well as in the grid-connected mode. In grid-connected mode PLL should be implemented based on measurements of the grid quantities in order to achieve synchronization of the generator with the grid.

IV. SIMULATION RESULTS
In order to facilitate the presentation of the results, a single realistic numerical simulation is conducted in MATLAB/Simulink programming environment. This simulation scenario is executed within 4 s time span and it includes a variable rotor speed, a change of output voltage set point, as well as a change of the generator load. The effectiveness and quality of this controller will have been carried out through comparison with the cascaded PI controller structure illustrated in Fig. 6. Furthermore, a comparison of our control approach was performed with the control structure presented in [36], which involves PI controller extended by feedforward part (PI+FF) in each control loop.
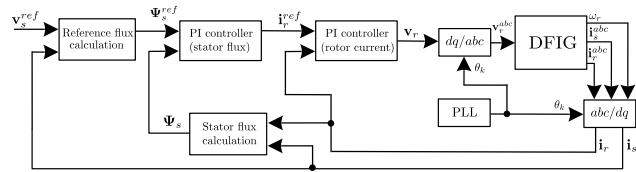
FIGURE 6. Implemented conventional cascaded PI control scheme.

The optimal parameters of the control structure (Fig. 6) and structure presented in [36] were tuned using MATLAB/Simulink ® function PID Tune. These obtained values for the proportional and integral gains of the four PI controllers (2 in each control loop for controlling d and q component of the stator flux and rotor current) are listed in Table 3 and Table 4 of the appendix. The obtained gains values for the cascaded PI as well as PI+FF control schemes are respectively listed In Table 3 and 4.

The primary control objective is to maintain stable amplitude and frequency of the generated stator voltage. During the simulation, the frequency set point is chosen to be 50 Hz. Initial reference for the per-phase stator voltage amplitude is set to 230 V and it changes to 210 V after 1 s. Fig. 7 depicts the variable rotor shaft speed ω_r for which the simulation was performed.

The proposed control system for DFIG also involves two observers with the same structure. The first is used to estimate $\mathbf{v}_r^{dist}$ term, while the second one estimates $\mathbf{i}_r^{dist}$. The estimation of the disturbance terms, are performed on the basis of applied system reference, rotor shaft speed, and stator load, which are time-varying quantities. The obtained estimation results are shown in Figs. 8-11, from which can be concluded that good estimations of the disturbance terms are achieved. It means
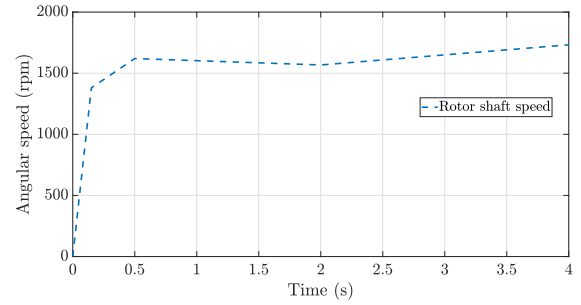
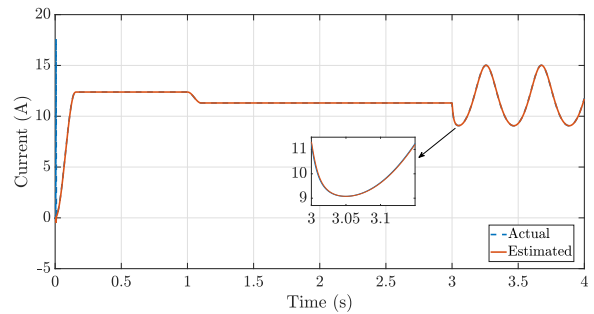**FIGURE 7.** The profile of mechanical angular speed of the rotor shaft.

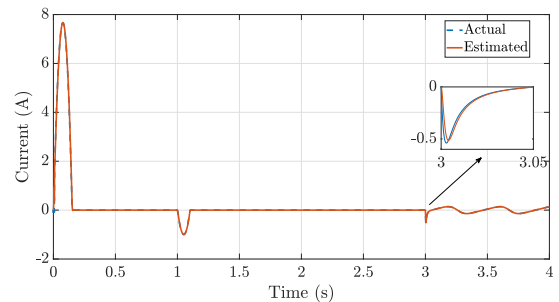**FIGURE 8.** Actual i_{rd}^{dist} and estimated $\hat{i}_{rd}^{dist}$ values of disturbance term.

FIGURE 9. Actual i_{rq}^{dist} and estimated $\hat{i}_{rq}^{dist}$ values of disturbance term.
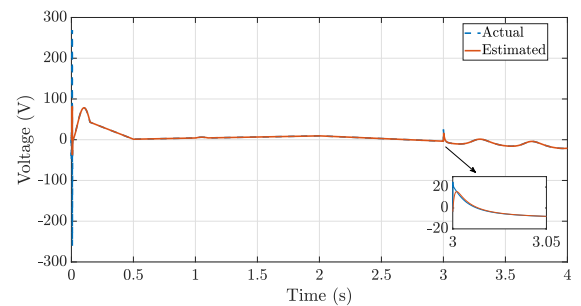
FIGURE 10. Actual v_{rd}^{dist} and estimated $\hat{v}_{rd}^{dist}$ values of disturbance term.

that deviations of the estimated from the actual disturbance terms are almost negligible.

The control performance of the inner loop controller is represented in Figs.12-15. It is obvious form these results that current controller in the inner loop is capable to efficiently control the rotor currents. Also, the obtained results indicate
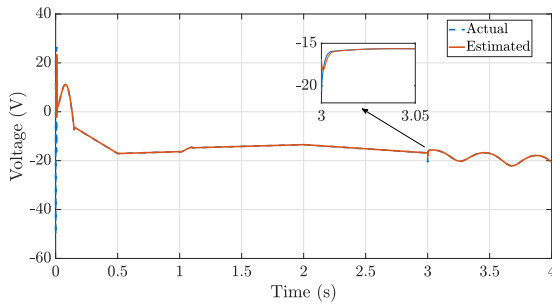
FIGURE 11. Actual v_{rq}^{dist} and estimated $\hat{v}_{rq}^{dist}$ values of disturbance term.
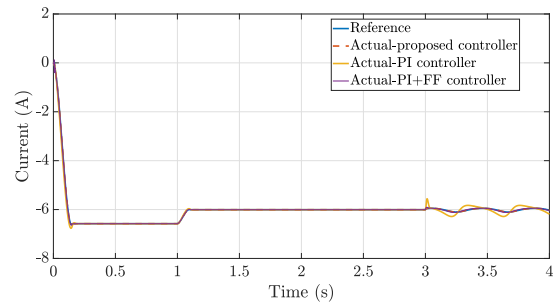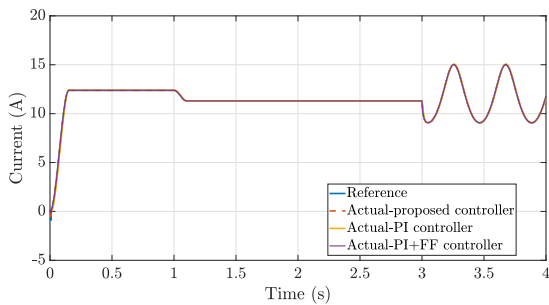

FIGURE 12. Actual and reference i_{rd}.

FIGURE 13. Tracking error for i_{rd}.

FIGURE 14. Actual and reference i_{rq}.

FIGURE 15. Tracking error for i_{rq}.

FIGURE 16. Three phase rotor voltage.

FIGURE 17. Actual and reference Ψ_{sd}.
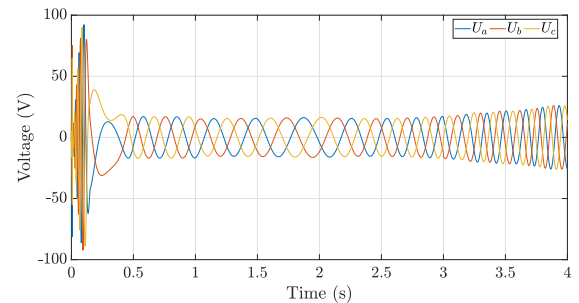
a very fast dynamic response of the inner loop which justifies utilization of the cascaded control structure. Therefore, the error between actual and reference i_{rd} and i_{rq} shown in Figs. 13 and 15 clearly indicates superior performance of the proposed structure in comparison with both PI and PI+FF control structure. Better transition as well as lower error in stationary state is especially notable in Figs. 13 and 15.

The time responses of the control rotor input voltages are given in Fig. 16. It is worth to note that values of these voltages are within rated nominal range, having smooth and expected waveform. Performance of the overall cascaded control structure can be assessed by analyzing results which are presented in Figs. 17-20. The proposed control structure provides successful tracking for the stator flux (both d and q components). This can be especially noted from Figs. 18 and 20. It is obviously clear that tracking error is significantly lower in comparison to the cascaded PI and PI+FF control structures. This is particularly evident in the simulation scenario when the stator load changes according to
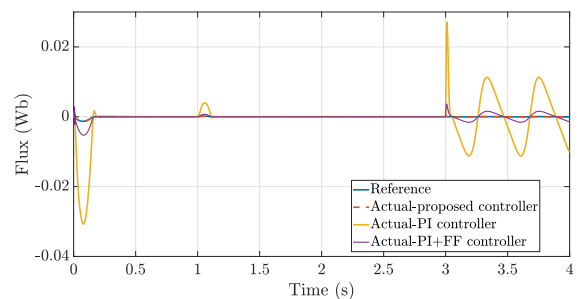
the sinusoidal law, as well as in stationary and transition. One can notice that Figs.17 and 18 are similar since reference of Ψ_{sd} is very close to zero, which means the error will be close to a negative value of Ψ_{sd}.

In order to compare effectiveness and efficiency of the proposed controller (PC) over the conventional cascaded PI and PI+FF control schemes, the mean absolute error (MAE)
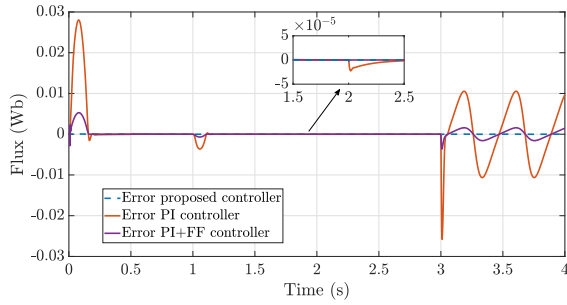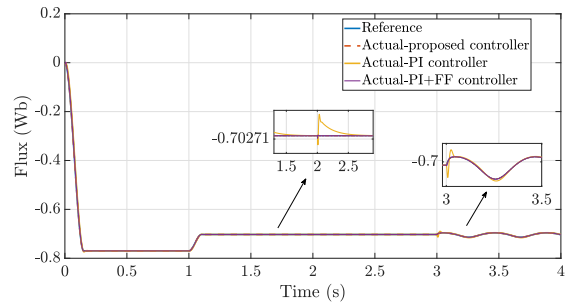
FIGURE 18. Tracking error for Ψ_{sd}.

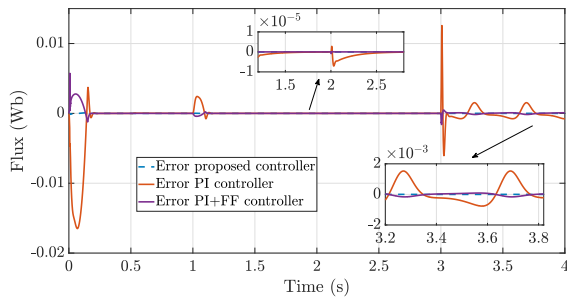**FIGURE 19.** Actual and reference Ψ_{sq}.

FIGURE 20. Tracking error for Ψ_{sq}.

TABLE 1. MAE comparison: proposed controller (PC) and cascaded PI control structure.

MAE	PC	PI	MAE decrease (%)
i_{rd} (A)	$1.0064 \cdot 10^{-4}$	0.0240	99.58
i_{rq} (A)	$2.5069 \cdot 10^{-5}$	0.0068	99.63
Ψ_{sd} (Wb)	$4.2409 \cdot 10^{-6}$	0.002	99.79
Ψ_{sq} (Wb)	$2.9551 \cdot 10^{-6}$	$6.5036 \cdot 10^{-4}$	99.55

is calculated taking into account four quantities i_{rd}, i_{rq}, Ψ_{sd}, Ψ_{sq}. Table 1 presents the MAE values for the proposed and cascaded PI control structure, while Table 2 gives a comparison of the MAE values of proposed controller and cascaded PI+FF. The MAE values are calculated within the time span from 0-4 s for all quantities. From all mentioned quantities the results represented in these tables indicate a significant decrease of the MAE values when we apply the proposed control approach.

The output stator voltages are shown in Fig. 21. The figure confirms that three phase sinusoidal voltages are generated at the output. Also one can note that the amplitude changes

TABLE 2. MAE comparison: proposed controller (PC) and cascaded PI+FF control structure.

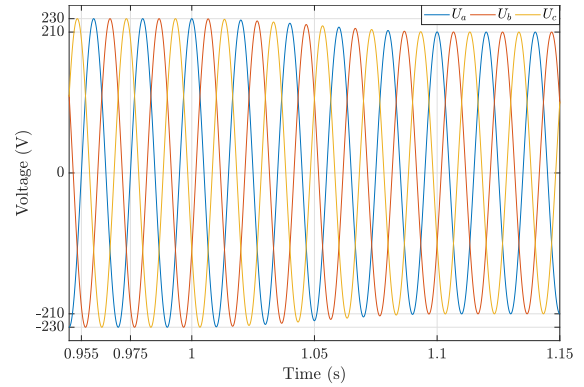| MAE	PC	PI+FF	MAE decrease (%)
i_{rd} (A)	$1.0064 \cdot 10^{-4}$	0.0024	95.81
i_{rq} (A)	$2.5069 \cdot 10^{-5}$	$7.3357 \cdot 10^{-4}$	96.58
Ψ_{sd} (Wb)	$4.2409 \cdot 10^{-6}$	$3.4402 \cdot 10^{-4}$	98.77
Ψ_{sq} (Wb)	$2.9551 \cdot 10^{-6}$	$9.9687 \cdot 10^{-5}$	97.04

FIGURE 21. Three phase stator voltage in stationary and transition phase (from 1 s to 1.1 s reference for the stator voltage amplitude changes from 230 V to 210 V).
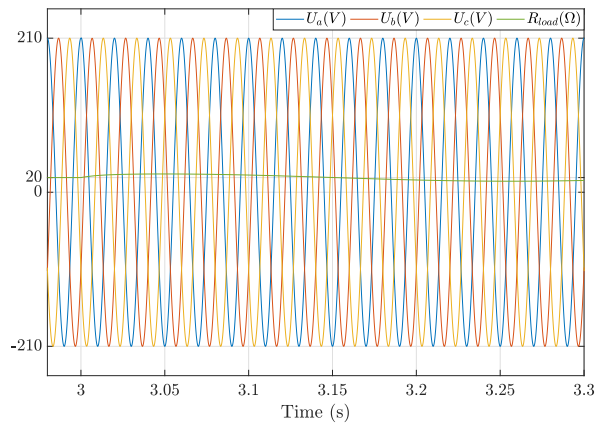

FIGURE 22. Three phase stator voltage when load changes (after 3 s the load starts to change around 20 Ω sinusoidally with amplitude of 5 Ω and frequency 15 $\frac{rad}{s}$).

smoothly and without notable overshoot from 230 V to 210 V. That response is according to the defined reference for the voltage amplitude. Also it can be seen that time interval from 0.955 s to 0.975 s contains one full period of the U_a stator voltage; thus, the output voltage frequency is equal to desired 50 Hz.

The variable speed profile of the mechanical angular speed of the rotor shaft, depicted in Fig.7 allows us to check the influence of the variable wind speed on the stability of the output frequency and voltage. As can be deduced from Figs. 22 and 23, the controller keeps the frequency constant regardless of the rotor speed change.

Moreover, these figures illustrate the time responses of the three-phase stator voltages when DFIG is subjected to
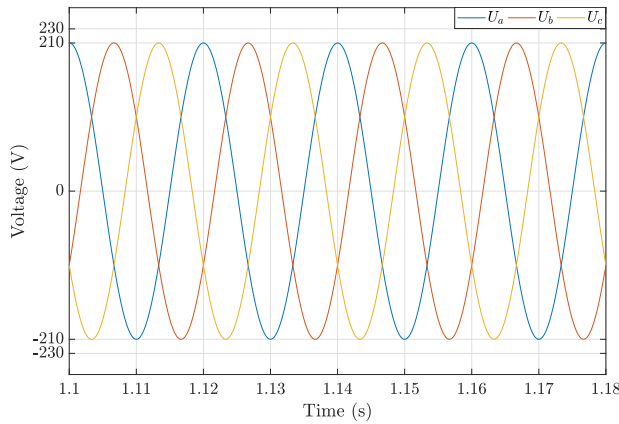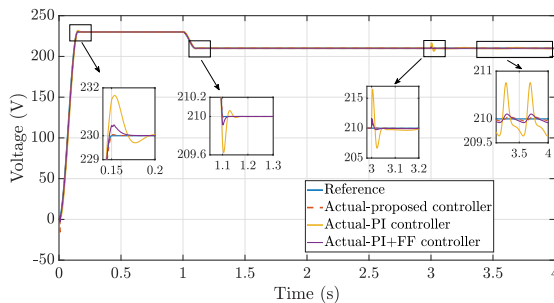
FIGURE 23. Three phase stator voltage.

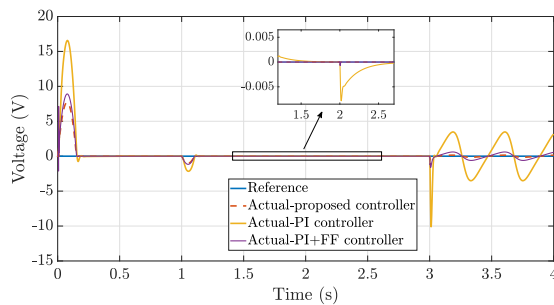**FIGURE 24. Comparison of the v_{sd} for considered control structures.**

FIGURE 25. Comparison of the v_{sq} for considered control structures.

load variations. It can be concluded that the variation of the load does not influence the amplitude and frequency of the stator voltages.

In order to additionally evaluate the control performance of the proposed controller, the time responses of the generated stator voltage for all considered control structures, presented in *dq* reference frame, are shown in Figs. 24 and 25. From the obtained results it can be concluded that proposed controller exhibits significantly better performance in tracking reference input, especially during the transient and steady state.

V. CONCLUSION AND FUTURE WORK
Stator voltage and frequency control for DFIG generator represents an important issue in wind power generation systems.

Our paper develops a novel control scheme for DFIG-based wind turbines in the island mode operation. It utilizes a cascaded structure with nominal plant controllers based on demanded error dynamics and disturbance observer in each control loop. The inner control loop is in charge of controlling the rotor currents, according to the references provided by the outer loop that controls the stator flux. The main task of the overall control system is to maintain stable voltage and frequency for the island mode operation of the DFIG generator where stator voltage is not determined by the utility grid. In general, this system is applicable in microgrid renewable energy generation systems. To evaluate the performance of the proposed control approach, it is compared with some concurrent control techniques, such as conventional cascaded PI structure and PI+FF control scheme. The proposed system exhibits significantly better performance during the transition process and notably smaller stationary error. This is related to the proposed DOB structure since the estimated disturbance term contains the varying load. Therefore, mentioned control systems are tested during a variable rotor speed as well as for several operating points of the generated voltage and variable load. Our system simultaneously ensures the stable and smooth operation of DFIG. Furthermore, the presented control system could be applied in the grid-connected mode only by changing the reference flux calculation, while keeping the entire structure the same, which provides it to be used in all possible operating modes of DFIG.

Future work would be towards considering nonlinear and unbalanced loads in the island mode operation. In addition, we plan to investigate the application of the proposed control structure both in grid-connected mode, as well as in the island mode. In addition, the proposed control algorithms will be verified by experiments as part of our future work.

APPENDIX
The data for the used three-phase wound rotor induction machine are: power 4 kW; nominal rotor speed 1410 rpm; nominal stator voltage Δ/Y 230/400 V Δ/Y; frequency 50 Hz; nominal stator current 15.2/8.8 A; $\cos\varphi = 0.83$; moment of inertia of the shaft 0.14 kgm²; nominal torque 27 Nm, nominal rotor voltage 100 V, nominal rotor current 25,5 A. Parameters of the machine's equivalent circuit are: $R_s = 1.025\,\Omega$, $R_r = 1.784\,\Omega$, $L_{s\sigma} = 8.97$ mH, $L_{r\sigma} = 8.97$ mH, $L_\mu = 0.117$ H.

Parameters of the four PI controllers that were used for comparison with the proposed controller are given in Table 3, while the gains of the PI controllers used in control structure with feedforward term are listed in Table 4.

TABLE 3. PI parameters.

	Proportional gain	Integral gain
i_{rd} controller	201.13	1001.34
i_{rq} controller	201.13	1001.34
Ψ_{sd} controller	10.38	4540.13
Ψ_{sq} controller	10.38	4540.13

TABLE 4. PI parameters for controller with feedforward term.

	Proportional gain	Integral gain
i_{rd} controller	7.76	16214.81
i_{rq} controller	7.76	16214.81
Ψ_{sd} controller	144.91	26976.68
Ψ_{sq} controller	144.91	26976.68

Parameters of the proposed controller are given in Table 5.

TABLE 5. Parameters of the proposed controller.

Parameter	Value
K_{rd}	8000
K_{rq}	8000
g_c	1200
K_{sd}	2000
K_{sq}	2000
g_s	1200

REFERENCES

[1] E. Rezaei, M. Ebrahimi, and A. Tabesh, "Control of DFIG wind power generators in unbalanced microgrids based on instantaneous power theory," *IEEE Trans. Smart Grid*, vol. 8, no. 5, pp. 2278–2286, Sep. 2017.

[2] R. Pena, R. Cardenas, G. M. Asher, J. C. Clare, J. Rodriguez, and P. Cortes, "Vector control of a diesel-driven doubly fed induction machine for a stand-alone variable speed energy system," in *Proc. IEEE 28th Annu. Conf. Ind. Electron. Soc. (IECON)*, vol. 2, Nov. 2002, pp. 985–990.

[3] S. Breban, M. Nasser, A. Ansel, C. Saudemont, B. Robyns, and M. Radulescu, "Variable speed small hydro power plant connected to AC grid or isolated loads," *EPE J.*, vol. 17, no. 4, pp. 29–36, Jan. 2008.

[4] W. Leonhard, *Control of Electrical Drives*. Berlin, Germany: Springer, 2001.

[5] J. A. Santisteban and R. M. Stephan, "Vector control methods for induction machines: An overview," *IEEE Trans. Educ.*, vol. 44, no. 2, pp. 170–175, May 2001.

[6] R. Pena, J. C. Clare, and G. M. Asher, "Doubly fed induction generator using back-to-back PWM converters and its application to variable-speed wind-energy generation," *IEE Proc., Electr. Power Appl.*, vol. 143, no. 3, pp. 231–241, 1996.

[7] R. Cardenas, R. Pena, S. Alepuz, and G. Asher, "Overview of control systems for the operation of DFIGs in wind energy applications," *IEEE Trans. Ind. Electron.*, vol. 60, no. 7, pp. 2776–2798, Jul. 2013.

[8] L. H. Hansen, L. Helle, F. Blaabjerg, E. Ritchie, S. Munk-Nielsen, H. Bindner, P. Sørensen, and B. Bak-Jensen, "Conceptual survey of generators and power electronics for wind turbines," Risø Nat. Lab., Roskilde, Denmark, Tech. Rep. 1205 (EN), 2001, pp. 71–73, vol. 1205.

[9] H. Li, Z. Chen, and H. Polinder, "Optimization of multibrid permanent-magnet wind generator systems," *IEEE Trans. Energy Convers.*, vol. 24, no. 1, pp. 82–92, Mar. 2009.

[10] H. Akagi and H. Sato, "Control and performance of a doubly-fed induction machine intended for a flywheel energy storage system," *IEEE Trans. Power Electron.*, vol. 17, no. 1, pp. 109–116, Jan. 2002.

[11] M. Esmaeeli, R. Kianinezhad, and M. Razzaz, "Field oriented control of DFIG in wind energy conversion systems," *J. Basic Appl. Sci. Res.*, vol. 2, no. 11, pp. 11486–11493, 2012.

[12] L. Djilali, E. N. Sanchez, and M. Belkheiri, "Neural sliding mode field oriented control for DFIG based wind turbine," in *Proc. IEEE Int. Conf. Syst., Man, Cybern. (SMC)*, Oct. 2017, pp. 2087–2092.

[13] S. Li, T. A. Haskew, K. A. Williams, and R. P. Swatloski, "Control of DFIG wind turbine with direct-current vector control configuration," *IEEE Trans. Sustain. Energy*, vol. 3, no. 1, pp. 1–11, Jan. 2012.

[14] N. R. N. Idris, C. L. Toh, and M. E. Elbuluk, "A new torque and flux controller for direct torque control of induction machines," *IEEE Trans. Ind. Appl.*, vol. 42, no. 6, pp. 1358–1366, Nov./Dec. 2006.

[15] T. Noguchi, H. Tomiki, S. Kondo, and I. Takahashi, "Direct power control of PWM converter without power-source voltage sensors," *IEEE Trans. Ind. Appl.*, vol. 34, no. 3, pp. 473–479, May 1998.

[16] G. Escobar, A. M. Stankovic, J. M. Carrasco, E. Galván, and R. Ortega, "Analysis and design of direct power control (DPC) for a three phase synchronous rectifier via output regulation subspaces," *IEEE Trans. Power Electron.*, vol. 18, no. 3, pp. 823–830, May 2003.

[17] M. Malinowski, M. P. Kazmierkowski, S. Hansen, F. Blaabjerg, and G. D. Marques, "Virtual-flux-based direct power control of three-phase PWM rectifiers," *IEEE Trans. Ind. Appl.*, vol. 37, no. 4, pp. 1019–1027, Jul./Aug. 2001.

[18] G. Abad, M. A. Rodriguez, G. Iwanski, and J. Poza, "Direct power control of doubly-fed-induction-generator-based wind turbines under unbalanced grid voltage," *IEEE Trans. Power Electron.*, vol. 25, no. 2, pp. 442–452, Feb. 2010.

[19] D. Santos-Martin, J. L. Rodriguez-Amenedo, and S. Arnalte, "Direct power control applied to doubly fed induction generator under unbalanced grid voltage conditions," *IEEE Trans. Power Electron.*, vol. 23, no. 5, pp. 2328–2336, Sep. 2008.

[20] L. Xu and P. Cartwright, "Direct active and reactive power control of DFIG for wind energy generation," *IEEE Trans. Energy Convers.*, vol. 21, no. 3, pp. 750–758, Sep. 2006.

[21] R. Datta and V. Ranganathan, "Direct power control of grid-connected wound rotor induction machine without rotor position sensors," *IEEE Trans. Power Electron.*, vol. 16, no. 3, pp. 390–399, May 2001.

[22] D. Zhi and L. Xu, "Direct power control of DFIG with constant switching frequency and improved transient performance," *IEEE Trans. Energy Convers.*, vol. 22, no. 1, pp. 110–118, Mar. 2007.

[23] P. Li, L. Xiong, F. Wu, M. Ma, and J. Wang, "Sliding mode controller based on feedback linearization for damping of sub-synchronous control interaction in DFIG-based wind power plants," *Int. J. Electr. Power Energy Syst.*, vol. 107, pp. 239–250, May 2019.

[24] P. Li, J. Wang, L. Xiong, S. Huang, M. Ma, and Z. Wang, "Energy-shaping controller for DFIG-based wind farm to mitigate subsynchronous control interaction," *IEEE Trans. Power Syst.*, vol. 36, no. 4, pp. 2975–2991, Jul. 2021.

[25] R. D. Shukla and R. K. Tripathi, "A novel voltage and frequency controller for standalone DFIG based wind energy conversion system," *Renew. Sustain. Energy Rev.*, vol. 37, pp. 69–89, Sep. 2014.

[26] R. Pena, J. C. Clare, and G. M. Asher, "A doubly fed induction generator using back-to-back PWM converters supplying an isolated load from a variable speed wind turbine," *IEE Proc., Electr. Power Appl.*, vol. 143, no. 5, pp. 380–387, 1996.

[27] R. Nair and N. Gopalaratnam, "Stator flux based model reference adaptive observers for sensorless vector control and direct voltage control of doubly-fed induction generator," *IEEE Trans. Ind. Appl.*, vol. 56, no. 4, pp. 3776–3789, Jul./Aug. 2020.

[28] B. Hopfensperger, D. J. Atkinson, and R. A. Lakin, "Stator-flux-oriented control of a doubly-fed induction machine: With and without position encoder," *IEE Proc., Electr. Power Appl.*, vol. 147, no. 4, pp. 241–250, 2000.

[29] A. K. Jain and V. T. Ranganathan, "Wound rotor induction generator with sensorless control and integrated active filter for feeding nonlinear loads in a stand-alone grid," *IEEE Trans. Ind. Electron.*, vol. 55, no. 1, pp. 218–228, Jan. 2008.

[30] G. Iwanski and W. Koczara, "Sensorless direct voltage control of the stand-alone slip-ring induction generator," *IEEE Trans. Ind. Electron.*, vol. 54, no. 2, pp. 1237–1239, Apr. 2007.

[31] A. B. Ataji, Y. Miura, T. Ise, and H. Tanaka, "Direct voltage control with slip angle estimation to extend the range of supported asymmetric loads for stand-alone DFIG," *IEEE Trans. Power Electron.*, vol. 31, no. 2, pp. 1015–1025, Feb. 2016.

[32] L. Guo, D. Wang, L. Diao, and Z. Peng, "Direct voltage control of stand-alone DFIG under asymmetric loads based on non-singular terminal sliding mode control and improved extended state observer," *IET Electr. Power Appl.*, vol. 13, no. 7, pp. 958–968, Jul. 2019.

[33] K. C. Wong, S. L. Ho, and K. W. E. Cheng, "Direct voltage control for grid synchronization of doubly-fed induction generators," *Electr. Power Compon. Syst.*, vol. 36, no. 9, pp. 960–976, Aug. 2008.

[34] A. Thakallapelli, S. Kamalasadan, K. M. Muttaqi, and M. T. Hagh, "A synchronization control technique for soft connection of doubly fed induction generator based wind turbines to the power grids," *IEEE Trans. Ind. Appl.*, vol. 55, no. 5, pp. 5277–5288, Sep. 2019.

[35] D.-Y. Li, Q.-T. Shen, Z.-T. Liu, H. Wang, M. Ding, and F. Liu, "Auto-disturbance rejection control for the stator voltage in a stand-alone DFIG-based wind energy conversion system," in *Proc. 35th Chin. Control Conf. (CCC)*, Jul. 2016, pp. 5916–5919.

[36] S. Arnaltes, J. Rodriguez-Amenedo, and M. Montilla-DJesus, "Control of variable speed wind turbines with doubly fed asynchronous generators for stand-alone applications," *Energies*, vol. 11, no. 1, p. 26, Dec. 2017.

[37] P. C. Krause, O. Wasynczuk, S. D. Sudhoff, and S. Pekarek, *Analysis of Electric Machinery and Drive Systems*, vol. 2. Hoboken, NJ, USA: Wiley, 2002.

[38] K. Ohnishi, M. Shibata, and T. Murakami, "Motion control for advanced mechatronics," *IEEE/ASME Trans. Mechatronics*, vol. 1, no. 1, pp. 56–67, Mar. 1996.

ADNAN OSMANOVIĆ (Member, IEEE) received the B.Eng. and M.Eng. degrees in electrical engineering from the Faculty of Electrical Engineering—University of Sarajevo, Bosnia and Herzegovina, in 2012 and 2014, respectively. He is currently working as a Senior Teaching and a Research Assistant with the Faculty of Electrical Engineering—University of Sarajevo. His research interests include the control of renewable energy sources and smart grid.

TARIK UZUNOVIĆ (Senior Member, IEEE) received the B.Eng. and M.Eng. degrees in electrical engineering from the University of Sarajevo, Sarajevo, Bosnia and Herzegovina, in 2008 and 2010, respectively, and the Ph.D. degree in mechatronics from Sabanci University, Istanbul, Turkey, in 2015.

He is currently an Associate Professor with the Department of Automatic Control and Electronics, Faculty of Electrical Engineering, University of Sarajevo, Sarajevo. His research interests include control theory, motion control, robotics, and mechatronics.
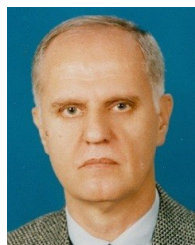
ASIF ŠABANOVIĆ (Life Senior Member, IEEE) received the B.S., M.S., and Dr. Eng. degrees in EE from the University of Sarajevo, Bosnia, and Herzegovina.

After graduation, he joined the Energoinvest-IRCA Sarajevo. He had been a Visiting Researcher at the IPU, Moscow; a Visiting Professor at Caltech, Pasadena, CA, USA; a Visiting Professor at Keio University, Yokohama, Japan; a Full Professor at Yamaguchi University, Ube, Japan; the Head of Robotics Department, Tubitak-MAM, Istanbul. He is currently an Emeritus Professor at the International University of Sarajevo and a member of the Academy of Sciences and Arts of Bosnia and Herzegovina. His research interests include control systems, motion control systems, robotics, mechatronics, and power electronics.

JASMIN VELAGIĆ (Member, IEEE) received the B.S. and M.S. degrees from the Faculty of Electrical Engineering and Computing, University of Zagreb, in 1995 and 1999, respectively, and the Ph.D. degree from the University of Sarajevo, in 2005. He is currently a Professor with the University of Sarajevo. His research interests include mobile robotics, motion planning and control, adaptive and robust control, and networked control.

• • •